Crossover from layering to island formation in Langmuir-Blodgett growth: Role of long-range intermolecular forces

Smita Mukherjee and Alokmay Datta*

Applied Material Science Division, Saha Institute of Nuclear Physics, 1/AF Bidhannagar, Kolkata 700 064, India

(Received 6 October 2010; published 7 April 2011)

Combined studies by atomic force microscopy, x-ray reflectivity, and Fourier transform infrared spectroscopy on transition-metal stearate (M-St, M = Mn, Co, Zn, and Cd) Langmuir-Blodgett films clearly indicate association of bidentate coordination of the metal-carboxylate head group to layer-by-layer growth as observed in MnSt and CoSt and partially in ZnSt. Crossover to islandlike growth, as observed in CdSt and ZnSt, is associated with the presence of unidentate coordination in the head group. Morphological evolutions as obtained from one, three, and nine monolayers (MLs) of M-St films are consistent with Frank van der Merwe, Stranski-Krastanov, and Volmer Weber growth modes for M = Mn/Co, Zn, and Cd, respectively, as previously assigned, and are found to vary with number (n) of metal atoms per head group, viz. $n = 1$ (Mn/Co), $n = 0.75$ (Zn), and $n = 0.5$ (Cd). The parameter n is found to decide head-group coordination such that $n = 1.0$ corresponds to bidentate and $n = 0.5$ corresponds to unidentate coordination; the intermediate value in Zn corresponds to a mixture of both. The dependence of the growth mode on head-group structure is explained by the fact that in bidentate head groups, with the in-plane dipole moment being zero, intermolecular forces between adjacent molecules are absent and hence growth proceeds via layering. On the other hand, in unidentate head groups, the existence of a nonzero in-plane dipole moment results in the development of weak in-plane intermolecular forces between adjacent molecules causing in-plane clustering leading to islandlike growth.

DOI: 10.1103/PhysRevE.83.041604 PACS number(s): 68.47.Pe, 78.30.Jw, 68.37.Ps, 61.05.cm

I. INTRODUCTION

Transition metals, due to the presence of highly directed orbitals of d electrons [1], show a number of coordinations, particularly in their bonding with organic functional groups [2]. For each of these coordinations there may again be more than one conformation due to different energy states corresponding to the alignment of d orbitals relative to the coordinate bonds [3]. This gives rise to polymorphism in such organometallic compounds [4]. Metal carboxylates are the simplest examples of these organometallics. But even in Langmuir-Blodgett (LB) multilayer growth [5] of divalent transition-metal carboxylates, different coordination between metal and carboxylate moieties in the head group is observed [6], depending on the particular transition metal employed.

If we look at the structure and morphology of these multilayers on hydrophilic substrates, some clear trends are observable. First, in all of them, molecules in the first layer, i.e., those in contact with substrate surface, have the metal-bearing head group touching the surface and both hydrocarbon chains (tails) pointing away from this surface. This gives rise to an asymmetric monolayer (AML) configuration. Second, in successive layers the molecules have a configuration where tails are placed symmetrically about the head group, corresponding to a symmetric monolayer (SML) configuration [7–11].

In order to understand the next interesting observation about these multilayers, it may be worthwhile to note that "pinhole defects" are a common surface defect that occurs, in particular, during manufacturing processes of one-dimensional periodic structures, such as in epitaxial growth of device-grade crystals, and may cause critical damage to the products based on such growth [12]. These defects are also common in Langmuir-Blodgett growth and, until recently, were supposed to be inherent in this growth process [13]. In general, these defects are expected to occur due to intermolecular forces becoming stronger and longer ranged than molecule-substrate forces. They are similar in nature to Volmer-Weber or island growth in heteroepitaxy in ultrahigh vacuum and, for similar reasons, i.e., when the lattice mismatch in the latter case is above a certain value, interatomic forces become stronger than the atom-substrate interaction. However, the relative importance of long-range forces is not apparent in heteroepitaxial growth.

It has already been shown that perfect i.e., "pinhole" defect-free growth can be achieved in LB growth of transition metal-bearing multilayers [9,14,15] under different experimental conditions. Specifically, from a comparative study of cadmium stearate and cobalt stearate LB multilayers, we have shown that it is possible to achieve perfect, i.e., "pinhole" defect-free multilayer growth by simply replacing Cd ion with Co ion in subphase [9]. Such defect-free growth is also reported to occur in cadmuim arachidate LB multilayers by raising the subphase pH [15]. In both cases, the head-group coordination of the system is found to change from unidentate to bidentate bridged. Moreover, not only coordination but rather a particular conformation of metal-bearing head group is required to grow defect-free multilayers for at least one of the transition-metal carboxylates (cobalt stearate) [16]. From these, and also from our previous work on the dependence of multilayer growth mode on head-group configuration in transition metal stearate LB films [17], a possible and perhaps more generalized basis of association of morphology with head-group coordination for this type of LB films is strongly hinted at. Results presented in this communication not only point to such general trends in atomic number of transition metal ion chosen but also

*alokmay.datta@saha.ac.in

explain the possible reasons behind such associations. It is observed that as atomic number of metal decreases, the number of metals per head group increases to unity, which crucially determines metal-carboxylate coordination and thus head-group structure. In doing so, the in-plane component of the head-group dipole moment is reduced to zero, which in turn drastically reduces in-plane intermolecular forces, allowing space filling to occur and hence promoting defect-free growth.

We have studied one-, three-, and nine-monolayer (ML) LB films of four different transition metal stearates viz. manganous stearate (MnSt), cobalt stearate (CoSt), zinc stearate (ZnSt), and cadmium stearate (CdSt). Of these, the Mn atom has all *d* orbitals occupied by one electron each (half-occupied), whereas both Zn and Cd atoms have fully occupied *d* orbitals. The Co atom has two *d* orbitals fully occupied and another three half occupied. Below Mn, i.e, when one of the *d* orbitals is unoccupied, divalent ions are not stable in solution and the LB deposition process is difficult to sustain. Using atomic force microscopy (AFM) [18] we have studied the morphological evolution of the films and compared them with different heteroepitaxial growth modes. The x-ray reflectivity (XRR) [19] technique was used to calculate electron density profiles (EDPs) across the films and also the number of metal ions per head group. Fourier transform infrared (FTIR) spectroscopy [20] was carried out to elucidate the metal-carboxylate coordinations.

II. EXPERIMENTAL DETAILS

One, three, and nine MLs each of CdSt, ZnSt, CoSt, and MnSt were deposited on hydrophilic silicon (100) substrate by use of the LB technique [21]. For this, respective divalent metal ions (i.e., Cd^{2+}, Zn^{2+}, Co^{2+}, and Mn^{2+}) were introduced in a Langmuir trough (KSV instruments, KSV-5000) containing Milli-Q water (resistivity 18.2 MΩ/cm) by addition of 0.5 mM chloride solutions of these. Subphase pH was maintained at 6.0 by adding sodium bicarbonate ($NaHCO_3$, Merck, 99%). Stearic acid ($C_{17}H_{35}COOH$, Sigma-Aldrich, 99%) solution (0.5 mg/ml) was spread to form the monolayer. Silicon substrates used for film deposition were hydrophilized by keeping them in a solution of ammonium hydroxide (Merck, 98%), hydrogen peroxide (Merck, 98%), and Milli-Q water (H_2O: NH_4OH: H_2O_2 2:1:1 by volume) for 10–15 min at 100° C. Films were deposited at a monolayer pressure of 30 mN/m at 19° C at a dipping speed of 3 mm/min by subsequent up-down strokes of substrate through the air/water interface, with the first layer being deposited by an upstroke of substrate from water to air through the interface. Drying time after first stroke was 10 min. Films were checked for reproducibility. AFM of all films were performed in tapping mode using Nanoscope IV (VEECO Inc.) with a silicon cantilever (force constant 40 N/m). Scans were performed over several regions of the films for different scan areas. XRR was done using a Versatile X-Ray Diffractometer (VXRD; Bruker AXS) with wavelength $\lambda = 1.54$ Å($Cu\ K_\alpha$ line). FTIR spectroscopy (Spectrum GX, Perkin-Elmer) was carried out in attenuated total reflectance (ATR) mode at a resolution of 4.0 cm^{-1}.

III. RESULTS AND DISCUSSION

A. Morphological evolution and growth modes of transition metal stearates

1. Atomic force microscopy results

AFM topographic images of one-ML, three-ML ($2 \times 2\ \mu m^2$), and nine-ML ($20 \times 20\ \mu m^2$) films of MnSt and CoSt with their corresponding height distributions (insets) are shown in Fig. 1. Those for ZnSt and CdSt are shown in Figs. 2 and 3, respectively. The AFM height distribution data (solid circles) have been fitted with a Gaussian function (solid line) such that all height values are obtained from the fitted peak positions. We have studied the morphological evolution of these films with repsect to (I) layer number and (II) atomic number of metal. We discuss them one after the other as follows.

(I) Morphological evolution with layer number: In order to study the morphological evolution with layer number for each *M*-St film, the morphology of one-ML film is compared with those of its three-ML and nine-ML counterparts. For example, one-ML films of MnSt [Fig. 1(a)] and CoSt [Fig. 1(d)] show unimodal distributions with peaks at 12 and 14 Å, respectively, denoting true monolayer features, with uniform coverage (calculated r.m.s. roughnesses are 2.0 and 3.5 Å, respectively). Again, three-ML films of MnSt [Fig. 1(b)] and CoSt [Fig. 1(e)] show the formation of a defect-free, smooth symmetric monolayer (SML) (r.m.s. roughness of 5 and 2 Å, respectively) on top of the first asymmetric monolayer (AML). Unimodal distributions show very few pinholes of SML thickness (35 Å for MnSt and 49 Å for CoSt). The nine-ML counterparts of MnSt [Fig. 1(c)] and CoSt [Fig. 1(f)] resemble morphologies of their one-ML and three-ML counterparts, having unimodal distribution peaks at 32 and 48 Å, respectively (r.m.s. roughnesses are 4.2 and 7.1 Å, respectively). Thus *surface morphology of MnSt and CoSt do not change with layer number* to at least four SMLs after the AML.

On the other hand, the surface morphology of one-ML ZnSt [Fig. 2(a)], which also shows a true monolayer feature (unimodal distribution peak at 32 Å and r.m.s. roughness 3.8 Å) is found to change with deposition of a SML on top of the AML as is evident from the 3ML ZnSt film [Fig. 2(b)]; morphology of the latter shows development of pinholes (height distribution showing islands of heights 23, 53, and 106 Å; with r.m.s. roughness of 16 Å). Surface morphology of nine-ML ZnSt film [Fig. 2(c)] resembles that of its three-ML counterpart and has a multimodal distribution of different heights (70, 94, 170, 193, and 206 Å). So the *surface morphology of ZnSt changes with layer number* such that island formation commences with deposition of first SML on the AML and continues to at least the next three SMLs.

Surface morphology of one-ML CdSt film [Fig. 3(a)] is found to differ drastically from the rest. In sharp contrast to the observed unimodal distributions of the one-ML depositions of the other three *M*-St films, one-ML CdSt comprises islands of various heights (62, 92, and 134 Å) as is evident from its multimodal distribution. The r.m.s. roughness estimated was 36 Å. Again, morphology of three-ML CdSt film [Fig. 3(b)] shows similar distribution with domainlike growth of various

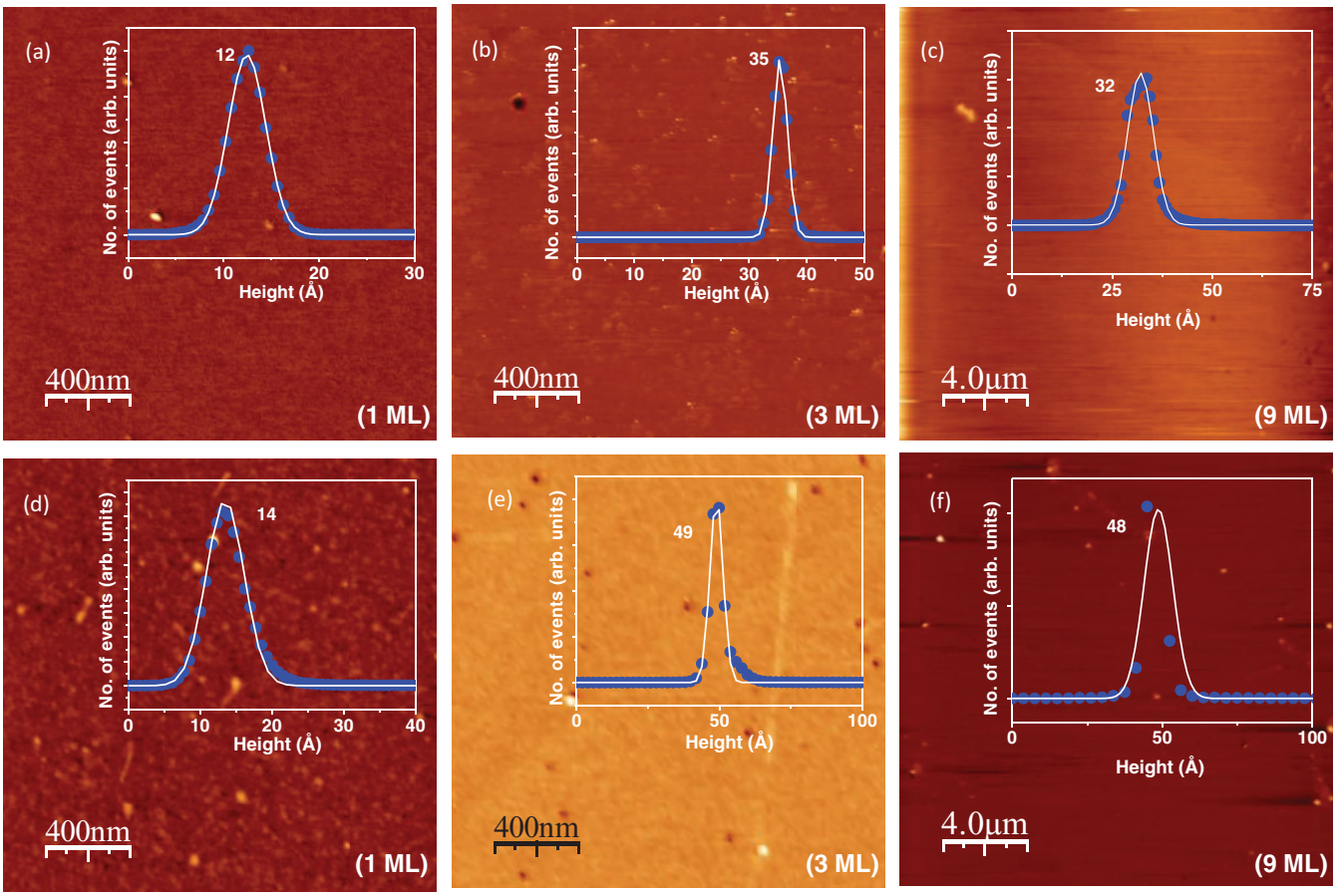

FIG. 1. (Color online) AFM topographic images of MnSt and CoSt films showing Frank Van der Merwe–type growth. In the figure, (a) and (d) represent one-ML ($2 \times 2\ \mu m^2$), (b) and (e) represent three-ML ($2 \times 2\ \mu m^2$), and (c) and (f) represent nine-ML ($20 \times 20\ \mu m^2$) films of [(a)–(c)] MnSt and [(d)–(f)] CoSt LB films with corresponding height distributions (inset). In all insets, height distribution data (plotted as dots) is fitted by Gaussian function (solid line).

heights (49, 112, and 142 Å) separated by dark ridges (r.m.s. roughness was 42 Å). Peak of height 49 Å denotes height of pinholes present on top of domains. The same was estimated separately (56 Å) from a smaller AFM scan ($200 \times 200\ nm^2$) of these portions only (not shown). Peak values obtained are close to those of one-ML CdSt distribution curve. This indeed shows that for three-ML CdSt film, deposition process is basically a continuation of 3D island formation. The nine-ML counterpart [Fig. 3(c)] is a continuation of the three-ML film with islands of various heights (62, 168, 203,, 223, and 243 Å). So, strictly speaking, there is *no change in the surface morphology of CdSt with layer number*, just as in MnSt and CoSt. Thus we see that under this classification of morphological variation with layer number, MnSt, CoSt, and CdSt fall into one group and ZnSt stands apart.

(II) Morphological evolution with atomic number of metal: Comparing the AFM results of all four metal stearates, we find that LB growth changes from 2D layering to commencement of 3D island formation with increase in atomic number (Z) of metal from Mn to Cd. Moreover, island formation starts from the first AML in CdSt but only from the first SML in ZnSt (after deposition of a smooth AML), whereas there are no island formations at all in MnSt or CoSt, where AMLs and SMLs show smooth morphology. Thus by studying their morphological evolution as regards commencement of island formation which depends on the atomic number of metal, the M-St films can be classified under the three growth modes observed in heteroepitaxy [22,23], viz. Volmer-Weber (VW) or growth by 3D island formation as in CdSt, Frank-Van der Merwe (FM) or growth via 2D layering as in MnSt and CoSt and Stranski-Krastanov (SK), where island formation follows 2D layer-by-layer growth, as in ZnSt. We have previously classified LB films under these three heteroepitaxial growth modes from fractal dimension analysis [17] and that classification system is consistent with our present direct results.

Thus, of the above two classifications, the second appears to be of greater interest as this classification resembles those observed in general heteroepitaxial growth and hence finds a broader footing. However, since AFM is a surface-sensitive technique, it does not provide the actual values of the thicknesses of the deposited layers; therefore, we have employed x-ray reflectivity to obtain information about the layer thickness and their corresponding coverage to confirm our classification of growth modes.

2. *X-ray reflectivity results*

X-ray reflectivity curves (open circles) of MnSt [Fig. 4(a)], CoSt [Fig. 4(c)], ZnSt [Fig. 4(e)], and CdSt [Fig. 4(g)] were

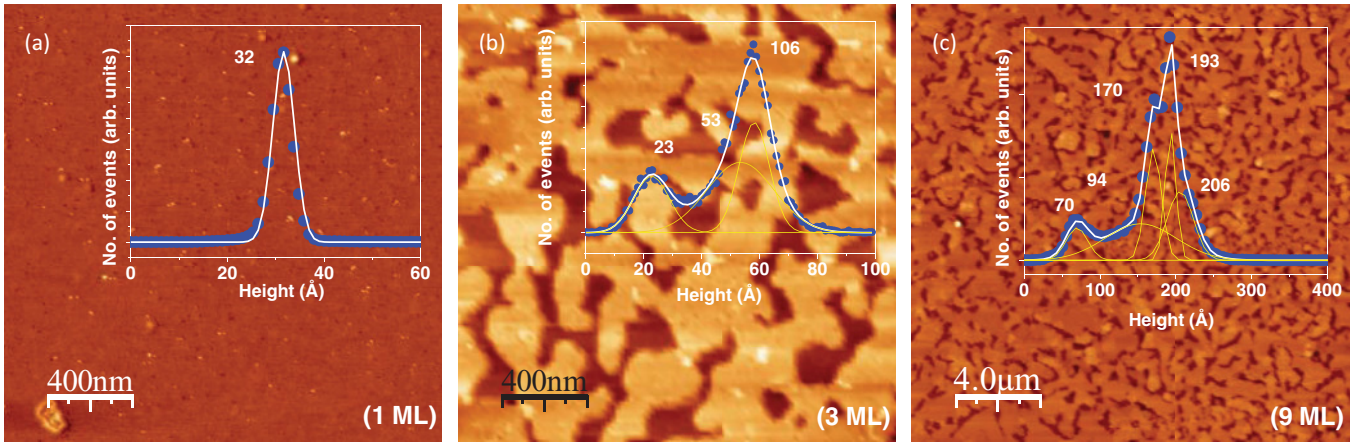

FIG. 2. (Color online) AFM topographic images of ZnSt films showing Stranski-Krastanov–type growth. In the figure, (a), (b), and (c) represent one-ML ($2 \times 2\ \mu m^2$), three-ML ($2 \times 2\ \mu m^2$), and nine-ML ($20 \times 20\ \mu m^2$) films, respectively, with their corresponding height distributions (inset). Height distribution data (plotted as dots) is fitted by a Gaussian function (solid line), where thick line represents composite fit and thin lines represent individual peak fits.

fitted (solid lines) using Parratt formalism [24], where each film is divided into layers of fixed thickness (d), average electron density (ρ), and interfacial roughness (σ) and used as fit parameters. Electron density profiles (EDPs) for films (ρ as a function of film thickness z, where $z = 0$ is air) were constructed from best-fit values consistent with physical acceptability. The EDPs of MnSt [Fig. 4(b)], CoSt [Fig. 4(d)], ZnSt [Fig. 4(f)], and CdSt [Fig. 4(h)] are plotted as 3D graphs. In each graph, the individual EDPs for one-ML, three-ML, and nine-ML films are plotted together to show the variation of ρ with layer number as well. It must be mentioned that fits were very sensitive to variations in head-group electron density ($\sim 0.01\ e/Å^3$) and thickness (~ 0.1 Å), which provided required selectivity in extracting EDPs. However, as the metal-containing head-group layer in contact with the substrate is convoluted with interfacial width (or roughness), it is almost impossible to distinguish these head groups in most EDPs.

As mentioned earlier, XRR data confirm assignments of growth modes by AFM analysis with more accurate information about depth profile. XRR profile and EDP of one-ML MnSt, CoSt, and ZnSt confirm their true monolayer features as the extracted film thicknesses were of typical monolayer values of 23 Å for MnSt, 22 Å for CoSt, and 21 Å for ZnSt. Thicknesses estimated from fitted data of three-ML films are 76 Å for MnSt, 75 Å for CoSt, and 63 Å for ZnSt, which correspond to a typical trilayer thickness denoting formation of a SML on the AML. EDPs of both three-ML and nine-ML films of MnSt and CoSt show no decrease in ρ with layer number, suggesting uniform coverage and hence growth by 2D layering (FM type).

EDP of three-ML ZnSt shows a SML of low ρ on top of the AML. This shows that coverage of SML is significantlyless than the first AML, hinting at commencement of island formation after the first monolayer. In nine-ML ZnSt film, coverage decreases with each SML, showing that island formation continues at least to nine ML. ZnSt thus shows SK-type growth.

An extra hump in the reflectivity profile of one-ML CdSt indicates presence of islands forming on top of the AML. EDP shows existence of a comparatively low-density SML on top of the AML along with two more SMLs of negligible electron density, which were necessarily incorporated to fit the reflectivity profile. Thickness to the first SML, obtained from fit, was 69 Å. Thickness of the film to the first two SMLs was 114 Å, whereas total film thickness was 158 Å. These thicknesses are in agreement with peaks obtained from AFM data, as mentioned earlier. XRR data of three-ML CdSt shows a trilayer feature of thickness 76 Å of hydrocarbon tail density ($0.22\ e/Å^3$) that is much higher than that of the same of its one-ML counterpart ($0.09\ e/Å^3$). Although presence of two SMLs on top of the trilayer feature is evident from the AFM morphology and distribution, due to their negligible electron densities, they were not incorporated into the XRR fits. The nine-ML film shows continuation of island formation with a decrease in ρ with layer number. AFM and XRR measurements of CdSt films confirm growth by 3D island formation or, more precisely, VW-type growth. Thus, XRR results are throughout in agreement with those obtained from AFM measurements, as regards evolution of morphology of M-St multilayers.

B. Dependence of film morphology on number of metal ions per head group

1. X-ray reflectivity results

Now, in order to find the reason behind the dependence of film morphology on atomic number of metal, the metal-bearing head group should be studied in details. From XRR data, we have calculated the number of electrons per head group. Details of such a head-group analysis are given elsewhere [17]. In brief, calculations on metal-bearing headgroups were carried out with fitted XRR data, assuming uniform molecular cross-sectional area A of 20 Å^2 [21]. The number of electrons N_H (N_T) in head (tail) for each layer of a film was calculated as $\rho_H A d_H$ ($\rho_T A d_T$), where suffix H (T) refer to head (tail). To eliminate the effect of porosity, the ratio $R_{\mathrm{Exp}} = N_H/N_T$ was computed for each layer. Values of R_{Exp} for all films are given in Table I. In addition, theoretical R values (R_{Th}) for all films

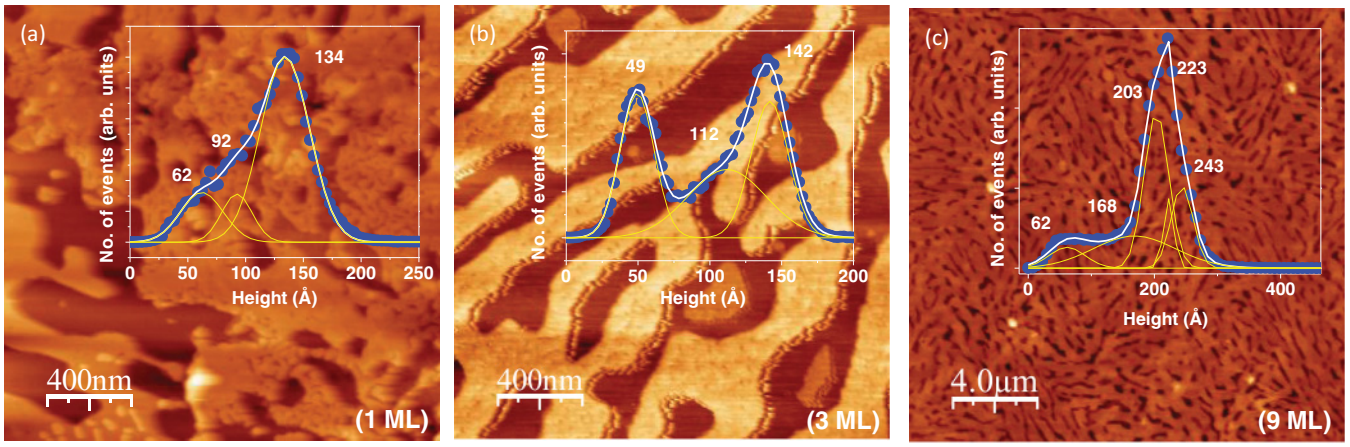

FIG. 3. (Color online) AFM topographic images of CdSt films showing Volmer-Weber–type growth. In the figure, (a), (b), and (c) represent one-ML ($2 \times 2\ \mu m^2$), three-ML ($2 \times 2\ \mu m^2$), and nine-ML ($20 \times 20\ \mu m^2$) films, respectively, with their corresponding height distributions (inset). Height distribution data (plotted as dots) is fitted by a Gaussian function (solid line), where the thick line represents composite fit and thin lines represent individual peak fits.

were calculated. Taking into account the symmetry of SMLs with respect to head and tails, and the lack of it in AML, an appropriate model of a molecule is constructed. With this model, R_{Th} was calculated for all films, varying the number of metal ions in model head groups such that R_{Th} values matched those of R_{Exp} ones. The total number of electrons in the model head group, for which R_{Th} was nearly equal to R_{Exp}, was thus estimated. From this, number of metal ions (n) per head group or carboxylate (COO) group is calculated for each layer in all deposited films. Results are given in Table I. In CoSt and MnSt, $n = 1.0$ for both the AML and SML head groups. However, in ZnSt, $n = 1.0$ for AML and $n = 0.75$ for the SML head group. In CdSt, R values matched well for $n = 0.5$ for both AML and SML. It is noted that for each layer, in all films, $n = 1.0$ corresponds to growth by layering, and for values less than 1.0, there is signature of island formation. We thus find that in deposition of each LB layer, for all M-St films, the morphology has a strong dependence on molecular configuration. Next, we try to find the cause behind such a dependence by elucidating the head-group structure.

TABLE I. Results of XRR analysis.

	AML				Successive SMLs			
M-St	Film	R_{Expt}	R_{Th}	n	Film	R_{Expt}	R_{Th}	n
CdSt	1ML	0.36	0.34	0.5	3ML (1)	0.66	0.56	0.50
	3ML	0.40	0.34	0.5	9ML (1)	0.78	0.67	0.50
	9ML	0.44	0.34	0.5	9ML (2)	0.84	0.67	0.50
					9ML (3)	0.81	0.67	0.50
					9ML (4)	0.79	0.67	0.50
ZnSt	1ML	0.26	0.19	1.0	3ML (1)	0.25	0.28	0.75
	3ML	0.38	0.32	1.0	9ML (1)	0.25	0.28	0.75
	9ML	0.18	0.19	1.0	9ML (2)	0.27	0.28	0.75
					9ML (3)	0.30	0.28	0.75
					9ML (4)	0.30	0.28	0.75
CoSt	1ML	0.30	0.30	1.0	3ML (1)	0.52	0.60	1.00
	3ML	0.26	0.30	1.0	9ML (1)	0.46	0.60	1.00
	9ML	0.24	0.30	1.0	9ML (2)	0.48	0.60	1.00
					9ML (3)	0.48	0.60	1.00
					9ML (4)	0.48	0.60	1.00
MnSt	1ML	0.25	0.28	1.0	3ML (1)	0.96	0.69	1.00
	3ML	0.38	0.28	1.0	9ML (1)	0.23	0.32	1.00
	9ML	0.11	0.16	1.0	9ML (2)	0.23	0.32	1.00
					9ML (3)	0.25	0.32	1.00
					9ML (4)	0.24	0.32	1.00

Now, the number of metal ions (n) per COO group calculated from XRR gives insight into the metal-carboxylate coordinations in the films. There are three types of metal-carboxylate coordinations: unidentate coordination, bidentate bridging coordination, and bidentate chelate coordination [25]. Unidentate coordination results from the contribution of a half metal per COO group, whereas bidentate coordinations (both bridge and chelate) have one metal per COO group. The values of n, as obtained from XRR, suggest that CoSt and MnSt prefer bidentate coordination in all layers, whereas CdSt prefers unidentate coordination. However, the situation is something of a combination in ZnSt. Whereas, in its AML, ZnSt would prefer bidentate coordination, the number of metal ions per head-group contribution in ZnSt SMLs suggests a mixture of coordinations in these layers.

2. *FTIR results*

In order to directly look at metal-carboxylate coordinations, FTIR spectroscopy in the ATR mode was carried out. FTIR spectra for (I) MnSt and (II) ZnSt are shown in Fig. 5(a). ATR measurements for CoSt and CdSt samples have been reported previously [9] and hence their spectra are not given here. To find the coordination of a metal ion with a carboxylate group, the differences in symmetric (ν_s) and asymmetric (ν_a) COO stretching frequencies (Δ) are measured [25]. These frequencies are separately shown for all four metal stearates [Fig. 5(b): (I) MnSt; (II) CoSt; (III) ZnSt, and (IV) CdSt].

For both MnSt (symmetric stretch at 1397 cm^{-1}, asymmetric stretch at 1541 cm^{-1}, and $\Delta = 144\ cm^{-1}$) and CoSt (symmetric stretch at 1397 cm^{-1}, asymmetric stretch at

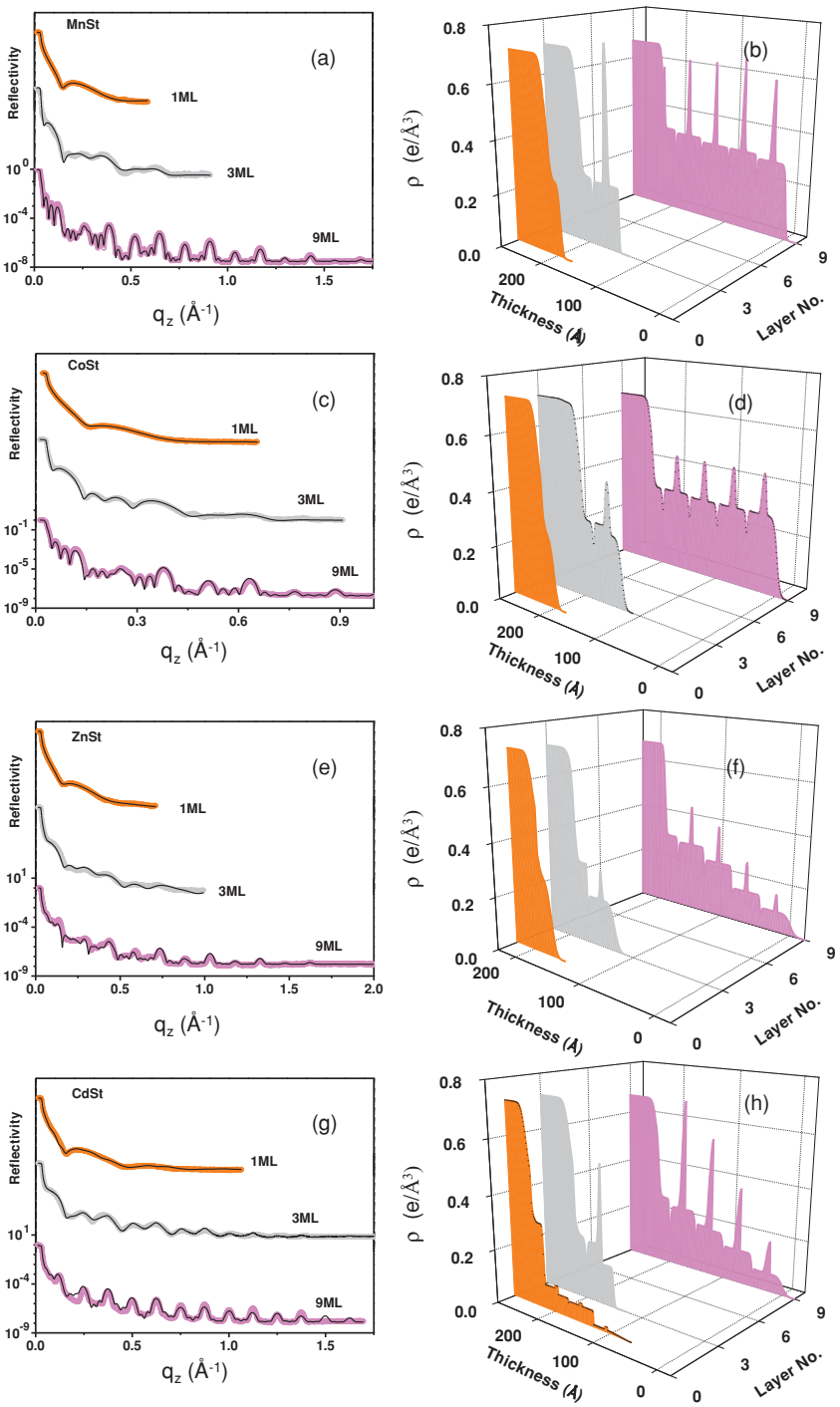

FIG. 4. (Color online) Reflectivity profiles (open circles) with fitted curves (solid lines) of (a) MnSt, (c) CoSt, (e) ZnSt, and (g) CdSt LB films. Curves for one ML and three MLs have been upshifted for clarity. Electron density profiles of (b) MnSt, (d) CoSt, (f) ZnSt, and (h) CdSt films plotted as 3D curves showing the variation of average electron density ρ with film thickness and layer number.

1540 cm^{-1}, and $\Delta = 143$ cm^{-1} [9]), coordination is bidentate bridged, consistent with $n = 1$. On the other hand, ZnSt shows the presence of two asymmetric stretches at 1538 and 1595 cm^{-1} and symmetric stretch at 1397 cm^{-1} giving $\Delta_1 = 141$ cm^{-1} and $\Delta_2 = 198$ cm^{-1}, thereby confirming existence of both bidentate bridged and unidentate coordinations. Equal intensity of peaks [Fig. 5(a) (II)] indicate that they are probably present in the same ratio, which gives an average contribution of three-quarter metal per carboxylate ion, i.e., $n = 0.75$. For CdSt, symmetric and asymmetric stretch bands are at 1397 and 1560 cm^{-1}, respectively, giving $\Delta = 163$ cm^{-1}, which corresponds to unidentate coordination [9] in which there are two carboxylate groups per metal ion.

Thus we find that the observed systematic variation of film morphology on the atomic number of metal stems from the association of bidentate coordination to growth by layering and unidentate coordination to island formation. Moreover, the formation of unidentate coordination in head groups can commence at any point of growth, wheereas island formation starts and continues to increase with layer number; the crossover from bidentate to unidentate is irreversible at least to nine MLs. Again, as mentioned, a trend is observed in the

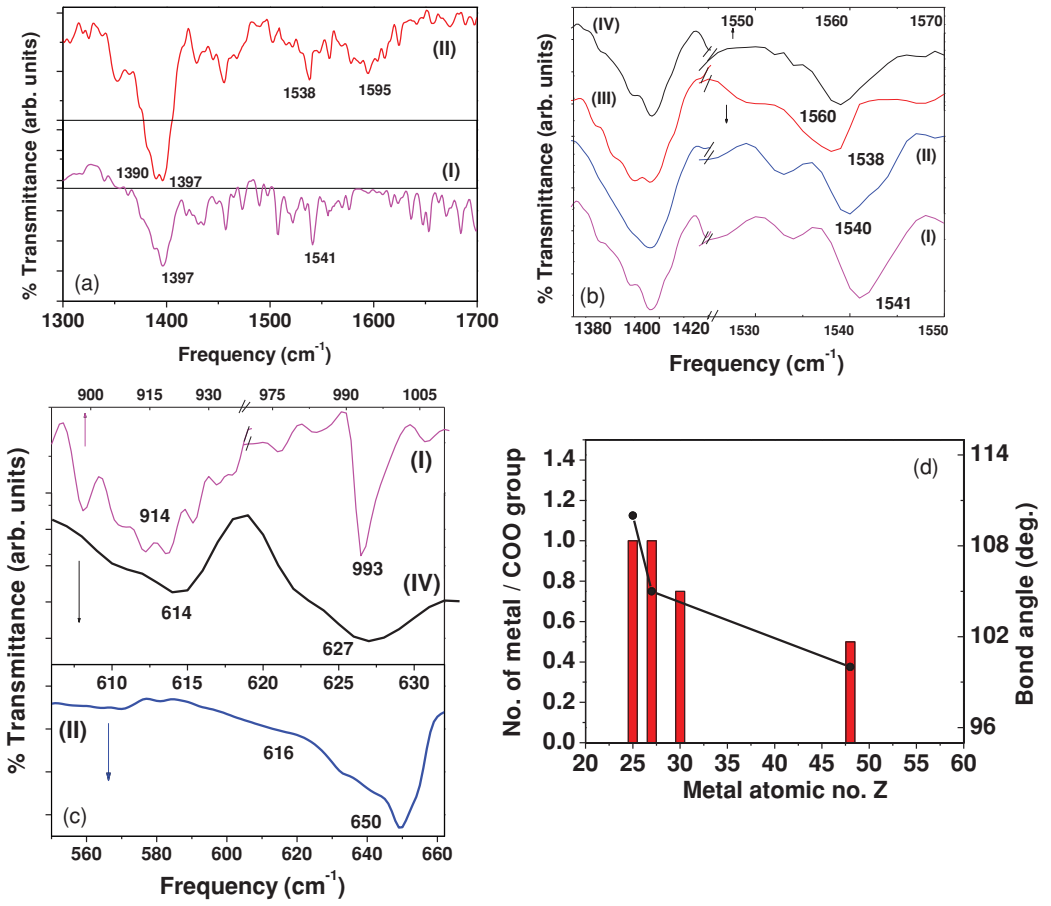

FIG. 5. (Color online) (a) FTIR spectra of (I) MnSt and (II) ZnSt; portions of spectra showing (b) COO and (c) O–M–O (M = Mn, Co, Zn, Cd) stretching frequencies for (I) MnSt, (II) CoSt, (III) ZnSt, and (IV) CdSt films. (d) Variation of the number of electrons (n) per COO group (shown as histogram) and metal carboxylate bond angle (plotted as points joined by line) with atomic number Z of metal for M-St films.

commencement of islandlike growth in moving toward a metal of a higher atomic number, as this leads to lower n.

Again, from AFM, XRR, and FTIR results, it is clear that a change in morphology with coordination can commence at any layer and so it can be postulated that coordination affects growth in the in-plane direction. The questions that come in mind are (i) How does head-group coordination affect in-plane growth and (ii) Why does coordination change when there is a change in the atomic number of the transition metal? In order to address the first question we have tried to construct suitable models for the bidentate and unidentate head groups, for both AML and SML from a knowledge of their structure and bonding obtained from XRR and FTIR, and tried to calculate the dipole moment of individual head groups in order to estimate the in-plane long-range forces between molecules. The answer to the second question comes as a logical follow-up. These are discussed in the next subsections.

At this point, we must mention that the oxygen-metal-oxygen bond angle has been extracted from the FTIR data based on metal-oxygen symmetric (ν_s) and asymmetric (ν_a) stretching frequencies. The details of such calculations are given elsewhere [16]. The assigned stretching frequencies for (I) MnSt, (II) CoSt, and (IV) CdSt are shown in Fig. 4(c). For MnSt ($\nu_a = 993\ \mathrm{cm}^{-1}$ and $\nu_s = 914\ \mathrm{cm}^{-1}$), the O–Mn–O bond angle is 110°; for CoSt ($\nu_a = 650\ \mathrm{cm}^{-1}$ and $\nu_s = 616\ \mathrm{cm}^{-1}$), the O–Co–O bond angle is 105°; and for CdSt ($\nu_a = 627\ \mathrm{cm}^{-1}$ and $\nu_s = 614\ \mathrm{cm}^{-1}$), the O–Cd–O bond angle is 100°, i.e., the O–M–O angle is found to decrease with an increase in metal atomic number. However, as ZnSt does not have a unique coordination, the conformation angle is also not unique and hence the bond angle for O–Zn–O is not determined. A plot of this bond angle, along with variation of n with atomic number Z of corresponding metal is shown in Fig. 5(d). A change in this angle may indicate a change in the hybridization state for these films [26] but a comparison with atomic structures of these transition metals leads us to conclude that there is no straightforward relation between the electronic structure of these metal atoms (in particular number of d electrons) and either the multilayer morphology or head-group coordination. We have, on the one hand, Mn and Co, which have differing numbers of d electrons, giving rise to identical coordination and LB morphology, and, on the other hand, Zn and Cd, which have the same number of d electrons, leading to different coordinations and morphologies. Nevertheless, an estimate of the O–M–O bond angles are necessary to determine the dipole moments of the head groups, as discussed in the next subsection.

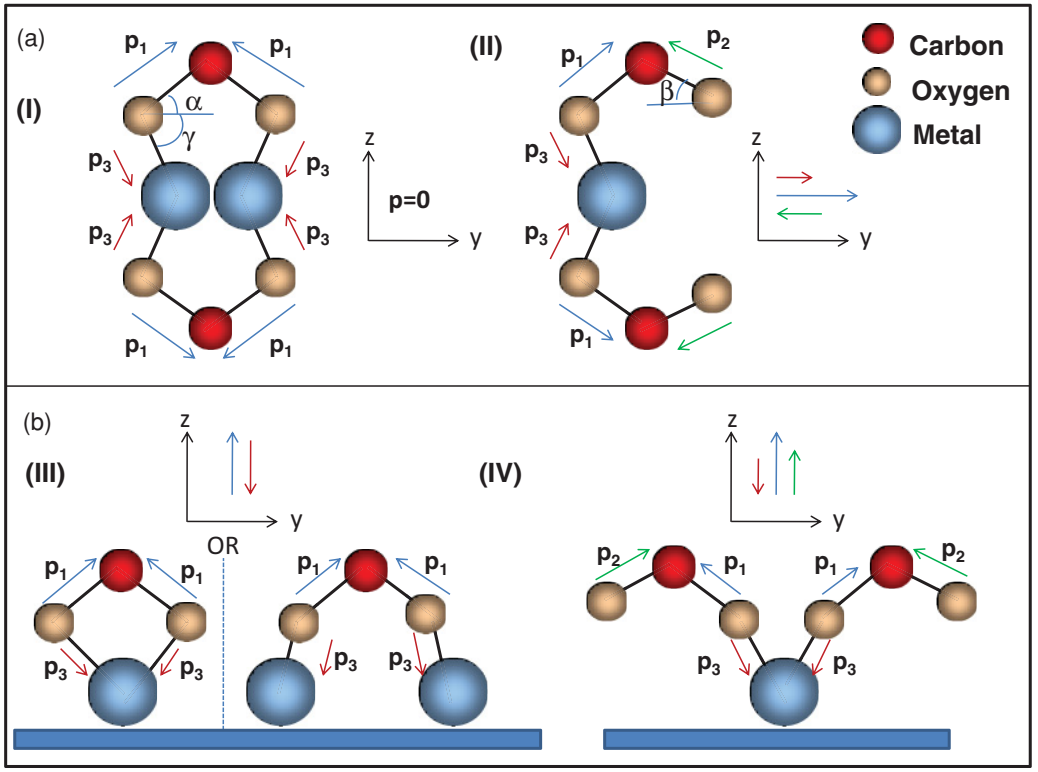

FIG. 6. (Color online) Constructed models for [(I) and (III)] bidentate and [(II) and (IV)] unidentate coordinated head groups in (a) SML and (b) AML of M-St films.

C. "Solid" and "liquid" like in-plane growth: Role of head-group dipole moment

As seen above, in all four M-St films, the head groups either have bidentate or unidentate coordinations. Moreover, the structure of the SML head groups [Fig. 6(a)] differs inherently from that of their AML counterparts [Fig. 6(b)]. For SML head groups, with a cross-sectional area of 20 Å^2 having a nonlinear O–M–O bond angle, possible structures for bidentate bridged (I) and unidentate (II) head groups are constructed. From NEXAFS studies of M-St films, it is reported [9] that in bidentate (unidentate) head groups the carboxylate group has equal (unequal) CO bond strength such that both COO groups are symmetric (asymmetric) in nature. In the case of bidentate head groups, two pairs of symmetric CO bonds leads to a contribution of zero dipole moment coming from the two carboxylate groups in the SML head group [Fig. 6(a) (I)]. Also, because the two O–M–O bonds are symmetric, giving a resultant of zero dipole moment, the net dipole moment of the bidentate SML head group is zero.

On the other hand, in unidentate head groups, asymmetric COO bonds cause a shift of the negative charge of the carboxylate ion toward the oxygen atom to which the metal ion is bonded, which causes the development of unequal dipole moments (e.g., p_1 and p_2) of the CO bonds in a COO group, as shown in Fig. 6(a) (II). Hence, the resultant dipole moment coming from the two COO groups is in the in-plane direction (y axis) and has a magnitude $p_{\mathrm{COO}} = 2(p_1\cos\alpha - p_2\cos\beta)$, where α (β) is the angle made with the y axis by the C–O bond, with is bonded (not bonded) to the metal ion. Again, since there is only one O–M–O linkage, its net dipole moment is also along the y axis and has a magnitude of $p_M = 2p_3\cos\gamma$, where p_3 is the dipole moment of an individual M–O bond and γ is the angle made by the M–O bond with the in-plane direction. Thus, in unidentate head groups, the net dipole moment is given by $p_{\mathrm{UC}} = p_{\mathrm{COO}} + p_M$ and acts totally in-plane.

As mentioned above, head-group structures [both bidentate (III) and unidentate (IV)] in AMLs [Fig. 6(b)] differ from those in SMLs. Here, for the bidentate configuration (both bridge and chelate), the net dipole moment is given by $p_B = 2(p_3\sin\gamma - p_1\sin\alpha)$, out-of-plane and toward the substrate. For an AML-unidentate head group, the net dipole moment has both in-plane as well as out-of-plane components. Whereas the out-of-plane component has a magnitude of $p_{\mathrm{out}} = 2(p_3\sin\gamma - p_1\sin\alpha - p_2\sin\beta)$ toward the substrate, the in-plane component p_{in} is the vector sum of the in-plane components of the dipole moments of the two COO groups (since they may not be coplanar) making the latter nonzero.

From a knowledge of the O–M–O bond angles, estimated from FTIR studies, and from the fact that both O–M bonds are symmetric, the angle γ is determined. Values of γ for CdSt, CoSt, and MnSt are 50°, 52.5°, and 55°, respectively. Taking p_3 as the difference in the electronegativity values of oxygen and metal, the values of p_M are calculated to be 2.25 D for CdSt, 1.90 D for CoSt, and 2.17 D for MnSt. Since the O–M–O linkage is not known, the value of p_M for ZnSt could not be calculated. Again, since the values of the angles α and β cannot be obtained from our studies, it is not possible to estimate p_{COO} and hence p_{UC} in our case. Even a theoretical estimate of p_{UC} cannot be given, as the angle between the O–M–O linkage

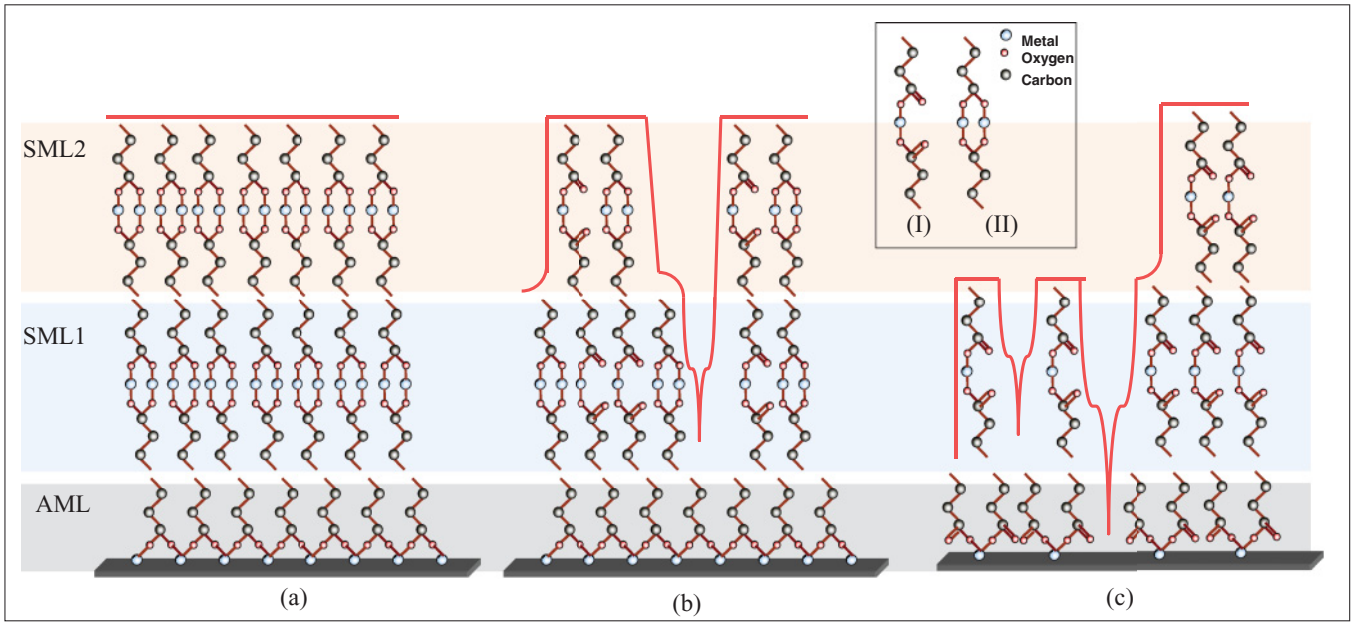

FIG. 7. (Color online) Different growth modes and coordinations in deposited films: (a) Frank van der Merwe type in MnSt/CoSt, (b) Stranski-Krastanov in ZnSt, and (c) Volmer-Weber in CdSt. The coordinations are separately shown (inset) as (I) unidentate and (II) bidentate bridged. The film surface morphology is shown by the red bold line.

and the O−C–O linkage (which lie in different planes) [16] is also not known.

Nevertheless, it is found that in both AML and SML head groups, the bidentate configuration has no in-plane component, whereas the unidentate configuration has a nonzero counterpart, the latter being quite appreciable, as suggested by the high value of p_M for CdSt. It is this nonzero in-plane component of the dipole moment arising in individual head groups that gives rise to in-plane intermolecular dipolar interactions among adjacent head groups, dictating their in-plane molecular growth. More specifically, due to dipole-dipole interactions between adjacent head groups, the unidentate system has stronger intermolecular attraction than molecule-substrate attraction, leading to domainlike growth with pinhole defects. In contrast, there exists no in-plane dipolar interactions in bidentate head groups, such that these molecules do not prefer clustering over growth by 2D layering. Moreover, in both types of AML head groups, there exists a nonzero component of dipole moment perpendicular to the substrate pointing toward it, which probably leads to adhesion of film to the substrate. However, in both types of SML head groups, there exists no component of the dipole moment in the out-of-plane direction, therefore dipolar interactions do not play a part in the formation of LB multilayers, the latter being solely governed by supramolecular tail-tail interactions of van der Waals and hyperconjugative origins, as we have suggested previously [27].

D. Dependence on the atomic number of metal

It is worthwhile mentioning that since, in bidentate head groups, the dipole moment of the system is, in general, lower compared to that of unidentate ones, the former is a much stabler system. It can thus be stated that transition-metal ions in general prefer to coordinate with the carboxylate groups as a bidentate bridge. In order to do so, it is necessary to accommodate an extra metal ion in the head group. With a decrease in the atomic number of the metal, the ionic radius decreases such that two metal ions can be accommodated in a head group only beyond a certain cut-off value (near Zn in our case). It is probably due to this that head-group coordination has a dependence on atomic number, which answers our second question.

It must be noted that this dependence of n on Z is basically limited to relatively lower pHs of the aqueous subphase on whose surface the Langmuir monolayers of stearic acid bond with the M ions dissolved in the subphase. The values of n can be manipulated with higher pH [15], and a bidentate-bridged head group with consequent pinhole-free growth can be achieved even for Cd ions, showing the crucial dependence of head-group coordination and LB growth mode on n.

As pointed out, the absence of head-group-to-head-group interactions in MnSt/CoSt SMLs, along with FM-type "fully wetting" films obtained from them, point to a "liquidlike" character of these layers, in particular, where molecules are in the symmetric configuration. It is to be noted that for preformed three-tailed amphiphiles, such as ferric stearate arranged in a similar fashion [28] or in the collapse of MnSt/CoSt monolayers on a water surface [8], a similar liquidlike behavior has been observed for the symmetric configuration. Again, the same islandlike growth was observed for CdSt SMLs [8] and here we have explained this growth as due to the in-plane intermolecular attraction. However, in-plane height correlations for CdSt show a "liquidlike" behavior at large length scales [29] and a self-affine behavior at short length scales [30]. Hence, similar studies need to be carried out on MnSt, CoSt, and ZnSt for comparison and these are underway.

IV. CONCLUSIONS

To conclude, morphological and structural studies clearly indicate that for at least four transition-metal stearate Langmuir-Blodgett (LB) films, viz. MnSt, CoSt, ZnSt, and CdSt, bidentate coordination of the metal-carboxylate head group gives rise to layer-by-layer growth as observed in Mn and Co and partially in Zn. Crossover to islandlike growth, as observed in Cd and Zn, is due to the presence of unidentate coordination in the head group. Morphological evolution of each M-St film is in accordance with its previously assigned growth mode, with MnSt/CoSt showing FM-type growth, ZnSt showing SK-type growth, and CdSt showing VW-type growth. Growth mode is found to vary with number (n) of metal atoms per head group, viz. $n = 1$ (MnSt/CoSt), $n = 0.75$ (ZnSt), and $n = 0.5$ (CdSt), which in turn decides head-group coordination such that $n = 1.0$ corresponds to bidentate and $n = 0.5$ corresponds to unidentate coordination; intermediate values in Zn correspond to a mixture of these coordinations. These results are summarized in Fig. 7. Moreover, it is found that in bidentate head groups, the in-plane dipole moment was zero, which causes intermolecular forces between adjacent molecules to be absent and hence allows growth to proceed via layering. On the other hand, in unidentate head groups, the existence of the nonzero in-plane dipole moment resulted in the development of weak in-plane intermolecular forces between adjacent molecules causing islandlike growth. Again, while in AML dipolar forces perpendicular to the substrate are found to exist in both head-group coordinations, and probably aid in metal-substrate adhesion, the same is found to be absent in all SMLs, suggesting that dipolar interactions arising in the head group do not affect LB multilayer formation. A gradual decrease in n, when going from Mn to Cd, suggests that crossover from layering to island formation is not an abrupt process but rather systematic with the change in the atomic number of the metal. Moreover, it is argued that dependence on atomic number probably stems from the dependence of coordination on the ionic radius of the metal, the latter decreasing with the decrease in the atomic number.

The major new findings of this work are as follows: (i) The metal-carboxylate coordination of the head group in divalent transition element-bearing LB multilayers is decided by the maximum number of metal ions per head group, which in turn depends on the atomic number of the metal. No clear correlation or trend can be found between the d orbital structure of the metal and this coordination, though the coordination admittedly is the result of the presence of these electrons. (ii) The coordination controls the film morphology by deciding the dipole moment of the metal-bearing head group. In particular, the absence of the in-plane component of the dipole moment leads to a "liquidlike" behavior, whereas its presence gives rise to "solidlike" domains or islands in the in-plane direction. This observation may be generalized to molecular systems with or without long-range interactions, especially with pronounced anisotropy in the long-range force. We plan to extend the latter observation to explore in-plane correlations on the surface of these LB films and also to look at the dynamics of Langmuir monolayers bearing these two kinds of head group. These studies are underway.

ACKNOWLEDGMENTS

The authors gratefully acknowledge Professor Debabrata Ghose and Dr. Puneet Mishra for their time and support in carrying out AFM measurements and Professor Satyajit Hazra for availability of the VXRD facility in carrying out XRR measurements. S.M. acknowledges the Department of Atomic Energy, India, for support.

[1] L. Pauling, *The Nature of the Chemical Bond and the Structure of Molecules and Crystals: An Introduction to Modern Structural Chemistry* (Cornell University Press, Ithaca, NY, 1960).
[2] K. Nakamoto, *Infrared Spectra of Inorganic and Coordination Compounds* (Wiley & Sons, New York, 1963).
[3] J. O. Bockris and A. K. N. Reddy, *Modern Electrochemistry I: Ionics* (Plenum Press, New York, 1998).
[4] N. P. Kumar, S. S. Major, S. Vitta, S. S. Talwar, A. Gupta, and B. A. Dasannacharya, Colloid Surface A **257**, 243 (2005).
[5] M. C. Petty, *Langmuir-Blodgett Films: An Introduction* (Cambridge University Press, Cambridge, UK, 1996).
[6] A. Gericke, and H. Huhnerfuss, Thin Solid Films **245**, 74 (1994).
[7] M. K. Sanyal, M. K. Mukhopadhyay, M. Mukherjee, A. Datta, J. K. Basu, and J. Penfold, Phys. Rev. B **65**, 033409 (2002).
[8] S. Kundu, A. Datta, and S. Hazra, Langmuir **21**, 5894 (2005).
[9] S. Mukherjee, A. Datta, A. Giglia, N. Mahne, and S. Nannarone, Chem. Phys. Lett. **451**, 80 (2008).
[10] S. Kundu, Coll. Surf. A **348**, 196 (2009).
[11] A. Datta, S. Kundu, M. K. Sanyal, J. Daillant, D. Luzet, C. Blot, and B. Struth, Phys. Rev. E **71**, 041604 (2005).
[12] H.-D. Lin, and D.-C. Ho, Int. J. Adv. Manuf. Technol. **34**, 567 (2007).
[13] Th. Geue, M. Schultz, U. Englisch, R. Stommer, U. Pietsch, K. Meine, and D. Vollhardt, J. Chem. Phys. **110**, 8104 (1999).
[14] D. Y. Takamoto, E. Aydil, J. A. Zasadzinski, A. T. Ivanova, D. K. Schwartz, T. Yang, and P. S. Cremer, Science **293**, 1292 (2001).
[15] S. Kundu, A. Datta, and S. Hazra, Chem. Phys. Lett. **405**, 282 (2005).
[16] S. Mukherjee, A. Datta, A. Giglia, N. Mahne, and S. Nannarone, Langmuir **25**, 3519 (2009).
[17] S. Mukherjee, and A. Datta, Appl. Surf. Sci. **256**, 380 (2009).
[18] D. Sarid, *Scanning Force Microscopy* (Oxford University Press, New York, 1994).
[19] J. Daillant and A. Gibaud, *X-Ray and Neutron Reflectivity: Principles and Applications* (Springer, New York, 1999).
[20] B. C. Smith, *Fundamentals of Fourier Transform Infrared Spectroscopy* (CRC Press, New York, 1996).
[21] D. K. Schwartz, Surf. Sci. Rep. **27**, 241 (1997).

[22] I. Daruka and A. L. Barabási, Phys. Rev. Lett. **79**, 3708 (1997).
[23] J. H. Van der Merwe, Interface Sci. **6**, 225 (1998).
[24] L. G. Parratt, Phys. Rev. **95**, 359 (1954).
[25] K. Nakamoto, *Infrared and Raman Spectra of Inorganic and Coordination Compounds* (Wiley & Sons, New York, 1970).
[26] I. A. Nekrasov, S. V. Streltsov, M. A. Korotin, and V. I. Anisimov, Phys. Rev. B **68**, 235113 (2003).
[27] S. Mukherjee, and A. Datta, J. Nanosci. Nanotechnol. **9**, 5237 (2009).
[28] S. Kundu, A. Datta, M. K. Sanyal, J. Daillant, D. Luzet, C. Blot, and B. Struth, Phys. Rev. E **73**, 061602 (2006).
[29] J. K. Basu, and M. K. Sanyal, Phys. Rev. Lett. **79**, 4617 (1997).
[30] J. K. Basu, S. Hazra, and M. K. Sanyal, Phys. Rev. Lett. **82**, 4675 (1999).